Li *et al. Carbon Research* (2022) 1:16
https://doi.org/10.1007/s44246-022-00015-3

Carbon Research

ORIGINAL ARTICLE

Open Access

Recycling waste nickel-laden biochar to pseudo-capacitive material by hydrothermal treatment: roles of nickel-carbon interaction

Deping Li[1], Jing Ma[2], Huacheng Xu[3], Xiaoyun Xu[1], Hao Qiu[1], Xinde Cao[1,4] and Ling Zhao[1,4*]

Abstract

Biochar as an absorbent is used to remove heavy metals from industrial wastewater, while the disposal of the residual has received little attention. This study attempted to convert the waste Ni-laden biochar into the pseudo-capacitive materials by hydrothermal treatment, investigated the optimal temperature (90–180 °C) and Ni content (100 and 500 mg g^{-1}), and explored the role of Ni-C interactions in the formation of the pseudo-capacitive materials. The highest pseudo-capacitance of 386.7 F g^{-1} was obtained with the highest Ni content and the lowest temperature. The high temperature (180 °C) induced thicker lamellar crystal $Ni(OH)_2$, while thinner flower-like $Ni(OH)_2$ crystal was observed at 90 °C. Low temperature enabled the $Ni(OH)_2$ crystals to disperse homogeneously on the carbon surface. The infrared spectroscopy showed that Ni promoted the disappearance of functional groups, indicating the catalytic effect of Ni on carbon structure, which also benefited their recrystallization and mutual encapsulation. Moreover, a combination of X-ray diffraction and thermogravimetry verified that Ni inserted into biochar graphite layer and enlarged the layer distance. This study provides a strategy for transforming hazardous nickel-laden biochar into the capacitive material and reveals that nickel can amplify the graphite layer and improve the stability of biochar-based pseudo-capacitive material during the hydrothermal treatment.

Highlights

- Waste biochar with Ni adsorbed was reclaimed to produce the pseudo-capacitive materials by hydrothermal treatment.
- Lower temperature of 90 °C helped the formation of flower-like $Ni(OH)_2$ crystal with highest capacitance of 386.7 F g^{-1}.
- Ni inserted into biochar graphite layer, enlarged the layer distance and improved the stability of $Ni(OH)_2$ and carbon.

Keywords: Nickel-laden biochar, $Ni(OH)_2$ crystal, Hydrothermal treatment, Pseudo-capacitive material, Graphite layer

*Correspondence: wszhaoling@sjtu.edu.cn

[1] School of Environmental Science and Engineering, Shanghai Jiao Tong University, Shanghai 200240, China
Full list of author information is available at the end of the article

Graphical Abstract

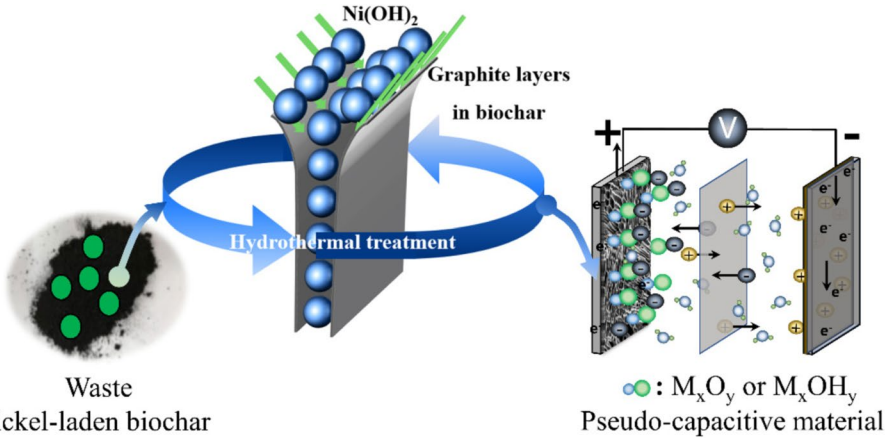

1 Introduction

Biochar produced from the pyrolyzation of organic biomass, always being 300–700 °C and O_2-starved atmosphere, has attracted wide attention of researchers in environmental application areas. It has broad applications as a low-cost heavy metal adsorbent and carbon sequestration material (Xue et al. 2012). In recent years, many studies focused on the application of biochar in the treatment of heavy metals contaminated industrial wastewater (Inyang et al. 2012; Kılıç et al. 2013; Joseph et al. 2019; Wang et al. 2019), and studies have proved that biochar has a rewarding adsorption capacity (87.15 mg g^{-1} and 115.2 mg g^{-1}) of nickel (An et al. 2019; Guo et al. 2020). However, the disposal or reuse of these waste biochar containing heavy metals has become a new challenge, and so far, there is no effective strategy to achieve large-scale recycling.

Researchers have attempted to convert these metals-laden carbon materials into electrochemical energy storage materials through microwave oxidation, direct carbonization, and KOH activation. The microwave oxidation can transfer Ni^{2+} to NiO and increase the Ni concentration in solid-phase from 16 mg g^{-1} to 55 mg g^{-1}, leading to a material with the capacitance of 123 F g^{-1} (at 5 mV s^{-1}) (Wang et al. 2017). However, the instability of NiOOH in KOH solution and the high solution resistance of NiO limit the practical applications of microwave oxidation (Huang et al. 2007). Researchers used direct carbonization at 800 °C to enhance the conductivity of carbon skeleton. With simultaneously transferred the adsorbed metal ions, Cr^{6+}, into metallic-carbon materials, they obtained capacitive materials with the capacitance of 122.5 F g^{-1} at 1 A g^{-1} (Hu et al. 2013) and 144.9 F g^{-1} at 2 mV s^{-1} (Hao et al. 2018). In addition, the H_2O_2 oxidation helped to enhance the capacitance of carbonized materials from 65 F g^{-1} to 265 F g^{-1} at 1 A g^{-1}, where $Mo_7O_{24}^{6-}$ had been loaded as the precursor for carbonization (Tao et al. 2014). Furthermore, our previous study used KOH activation to control the porous structure of nickel-laden biochar and produced a mesoporous carbon material (S_{BET} was 1181 m^2 g^{-1}) with a layer capacitance of 188.9 F g^{-1} at 0.5 A g^{-1} (Li et al. 2021). However, we found that it was not suitable to prepare layer capacitor (97.3 F g^{-1}) in the case of high metal concentration (500 mg g^{-1}).

The above efforts to improve the capacitance performance of metals-laden biochar show that there are still bottlenecks that limit the further increase of the capacitance of these materials. Firstly, the concentration of metal adsorbed by biochar is not high enough to meet the needs of producing high-performance capacitors. Secondly, the formation of the crystal structure of the adsorbed metal is not well controlled, so only the unevenly formed metal oxides on the surface of biochar contributes to the capacitance. Thirdly, it is difficult for the biochar bulk to participate in the electrochemical energy storage process, resulting in unsatisfactory electrochemical performance (Guo et al. 2013; Jiang et al. 2015). Moreover, as the lower conductivity of pure metal oxide/hydroxide (10^{-3}–10^{-2} S cm^{-1} for $NiO/Ni(OH)_2$) hinders its application (Zhang et al. 2019a), the introduction of carbon materials in metal oxide/hydroxide on the nanoscale has been widely explored for producing excellent capacitive materials (Patil et al. 2014; Sun et al. 2016; Makgopa et al. 2019). Simultaneously, the interaction between the metal and carbon skeleton affects

the electrical conductivity of the material, affecting the charge transfer impedance of the capacitive material (Cheng et al. 2021). The previous work has mentioned that the homogeneous combination of NiO nanoflake and graphene could contribute to high power density (138 Wh kg^{-1} at 5.25 kW kg^{-1}) (Wang et al. 2014).

Numerous studies have demonstrated that the hydrothermal recrystallization can control the formation of metal crystal structures, such as the shape or thickness of metal hydroxides (Yang et al. 2013, 2014). This method has been used to prepare the pseudo-capacitive materials of nickel hydroxide and high capacitances of 1450 F g^{-1} (at 5 A g^{-1}) and 2653.2 F g^{-1} (at 2 A g^{-1}) were attained (Tang et al. 2014; Jiang et al. 2015). However, few studies have been conducted to convert the waste metals-laden biochar into the capacitive material by the hydrothermal recrystallization, which distinguishes this study from others. In this system, according to the reference it hypotheses that metals would react with biochar organic functional groups and interact with carbon skeleton, with possible facilitation of secondary nucleation process and a subsequent promotion of uniformly dispersed metals crystallization (Lin et al. 2015).

Therefore, this study aimed to develop a hydrothermal method for recycling the waste metals-laden biochar into the capacitive materials with both the metals and the carbon structure fully utilized. We selected commonly industrial wastewater, electroplate water, which usually contains a high concentration of nickel ions (Cai et al. 2018), as the treatment objects. Biochar was used to adsorb Ni^{2+} from two simulated concentrations of Ni wastewater, and then the waste biochar was used to prepare the capacitive materials at different hydrothermal temperatures. The mechanisms relevant to the interaction of Ni and carbon were explored by instrumental analyses such as powder X-ray diffraction (XRD) and thermogravimetric analyses (TGA) to guide the regeneration of metal-laden biochar into high-quality capacitive materials.

2 Experimental section

2.1 The origin of waste nickel-laden biochar

This study selected traditional biomass, peanut shells, as the precursor to produce biochar. The peanut shell was collected from Shanghai, China. After being washed with deionized water, air-dried, and crushed, the peanut shell was placed into a pyrolysis system with a heating rate of 10 °C min^{-1} and a N_2 flow of 200 mL min^{-1}. The temperature was finally increased to 600 °C and held for 2 h (Li et al. 2021). The biochar product was named 'PS6'. The basic properties of the precursor and the biochar were exhibited in Table S1, which were measured with an elemental analyzer (Vario Macro Cube, Germany) and Brunauer-Emmete-Teller (BET, JW-BK222, JWGB, China).

Considering that the nickel content adsorbed on the surface of biochar should be the most important factor influencing the electrochemical properties of a material, this study firstly obtained biochars with different amounts of nickel absorbed by an alkali-carbon deposition. Our steps were: 0.5 g of PS6 was added to 500 mL $NiCl_2$ solution (made from $NiCl_2{\cdot}6H_2O$, Sinopharm Chemical Reagent Co., Ltd) with two concentrations (100 mg L^{-1} and 500 mg L^{-1} for Ni^{2+}), and the pH was slightly adjusted to 9.0 with KOH solution (Yonghua Chemical Technology Co., Ltd). Then the Ni-laden biochar was separated by filtration as the solid component (PS6-Ni1 and PS6-Ni5) for producing the capacitive material. In this step, adjusting the pH of wastewater to 9.0 could guarantee that all of the Ni^{2+} in wastewater would be deposited on the surface and pores of biochar as $Ni(OH)_2$. In the real industrial wastewater treatment process, adjusting the pH to 9.0 with alkali is an effective and commonly used strategy to guarantee the removal of almost all kinds of heavy metals.

2.2 Hydrothermal treatment

The solid components (PS6-Ni1 and PS6-Ni5) were dispersed into 20 mL deionized water, and the pH was adjusted to 7.0 with hydrochloric acid (Sinopharm Chemical Reagent Co., Ltd), then it's followed by ultrasonic treatment for 10 minutes. At this stage, the nickel was completely dissolved in the form of Ni^{2+} and dispersed into the solution. The pH of 7.0 could ensure that hydrochloric acid was exhausted, and would not affect the subsequent treatment.

Deionized water was added into the solution up to 80 mL, and the pH to 9.0 was adjusted with ammonia (Shanghai Titan Scientific Co., Ltd) drop by drop. After that, the solution was transferred to a 100 mL autoclave, and reacted at 90 °C, 120 °C, 150 °C and 180 °C for 4 hours (Tang et al. 2014). Then the system was cooled down naturally, and the collected materials were washed several times and dried at 60 °C. The samples were designated as PS6-Nix-Hy, where x represents the nickel concentration and y stands for the hydrothermal temperature, e.g., PS6-Ni1-H180 delegated the samples produced with nickel concentration of 100 mg g^{-1} and the hydrothermal temperature of 180 °C.

2.3 Electrochemical measurement

The electrochemical properties of the produced biochar-based pseudo-capacitive material were measured in a three-electrode system on an electrochemical workstation (Vertex. One, IVIUM, Netherlands) with Hg/HgO as the reference electrode,

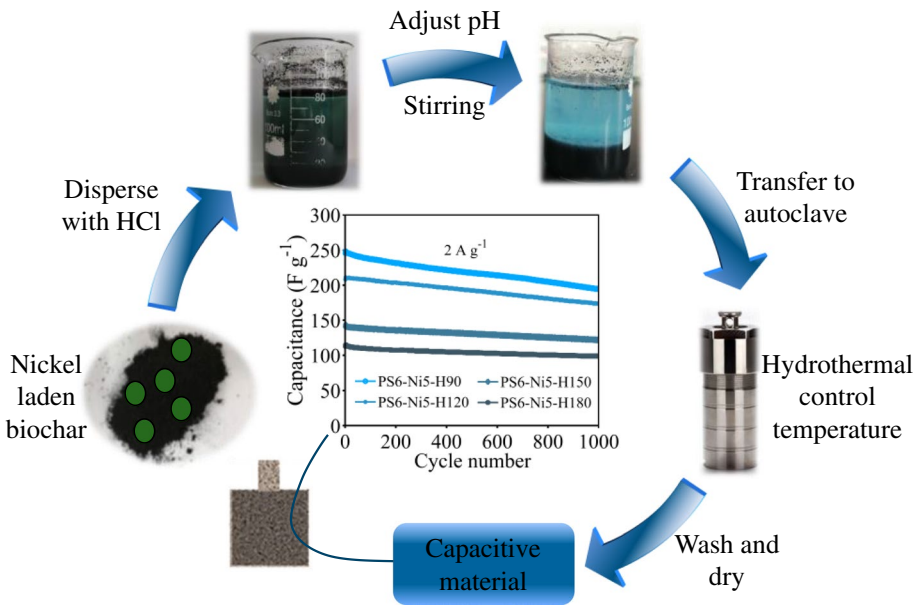

Fig. 1 Schematic illustration for the preparation of pseudo-capacitive materials from waste nickel-laden biochar

platinum plates as the counter electrode, and 1 M KOH as electrolyte. This method has been reported in our previous work, including the details of the electrode system and the preparation of the working electrode (Li et al. 2021).

Cyclic voltammetry (CV) curves were conducted at 5 mV s^{-1} from 0.1 V to 0.65 V, indicating the main pseudo-capacitance reaction of $Ni(OH)_2$ and capacitive performance (Tang et al. 2014; Jiang et al. 2015). The electric discharge curves directly exhibit the potential platform of the material to store electric energy (Hao et al. 2018; Nwanya et al. 2019), the capacitance, and the applicable current density. The electric discharge performances of the pseudo-capacitive materials were measured under different current densities and the capacitance was obtained in the three-electrode system by the following equation:

$$Cp = \frac{I\Delta t}{m\Delta V}$$

Where I (A) is the applied current, m (g) is the mass of sample, Δt (s) refers to the time of discharging and ΔV (V) represents the potential window (Zhi et al. 2013; Jia et al. 2019). The electrochemical impedance spectroscopy (EIS) exhibits the conductivity of the electrode, the electron transfer resistance of the electrode - electrolyte interface, and the mass transfer resistance of the electrolyte (Murali et al. 2019). The EIS was measured from 0.01 Hz to 100 kHz with the potential of 5 mV (Yang et al. 2018).

The preparation of the pseudo-capacitive materials from waste nickel-laden biochar and the prepared electrodes can be found in Fig. 1. Similar to the layer capacitive materials (Li et al. 2021), it is necessary to know whether the concentration of heavy metals and temperature will affect the structure and performance of the final materials during the hydrothermal process.

2.4 Exploring the nickel-carbon interaction

The Powder X-ray Diffraction (XRD, D/max-2200/PC, Rigaku, Japan) equipped with Cu Kα (λ = 1.540598 Å) was applied to probe the structure of $Ni(OH)_2$ crystal from 10° to 80° at a scanning rate of 2° min^{-1}. The functional groups of biochar and nickel carbon interaction were measured by Fourier Transform Infrared spectroscopy (FTIR, Prestige 21 FTIR, Shimadzu, Japan) and X-ray photoelectron spectroscopy (XPS, Kratos AXIS Ultra DLD, Shimadzu, Japan). The morphology of the materials was observed via scanning electron microscope (SEM, TESCAN-MAIA 3 GMU model 2016/ WITec apyron, Czech). Besides, thermogravimetric analysis (TGA, DSC1/1600HT, Mettler Toledo, Switzerland) was performed to study the thermal stability of $Ni(OH)_2$ crystals and the combustion process of carbon structure at temperatures ranging from 30 °C to 600 °C under air atmosphere, which could reflect the combination of $Ni(OH)_2$ and biochar after the hydrothermal process.

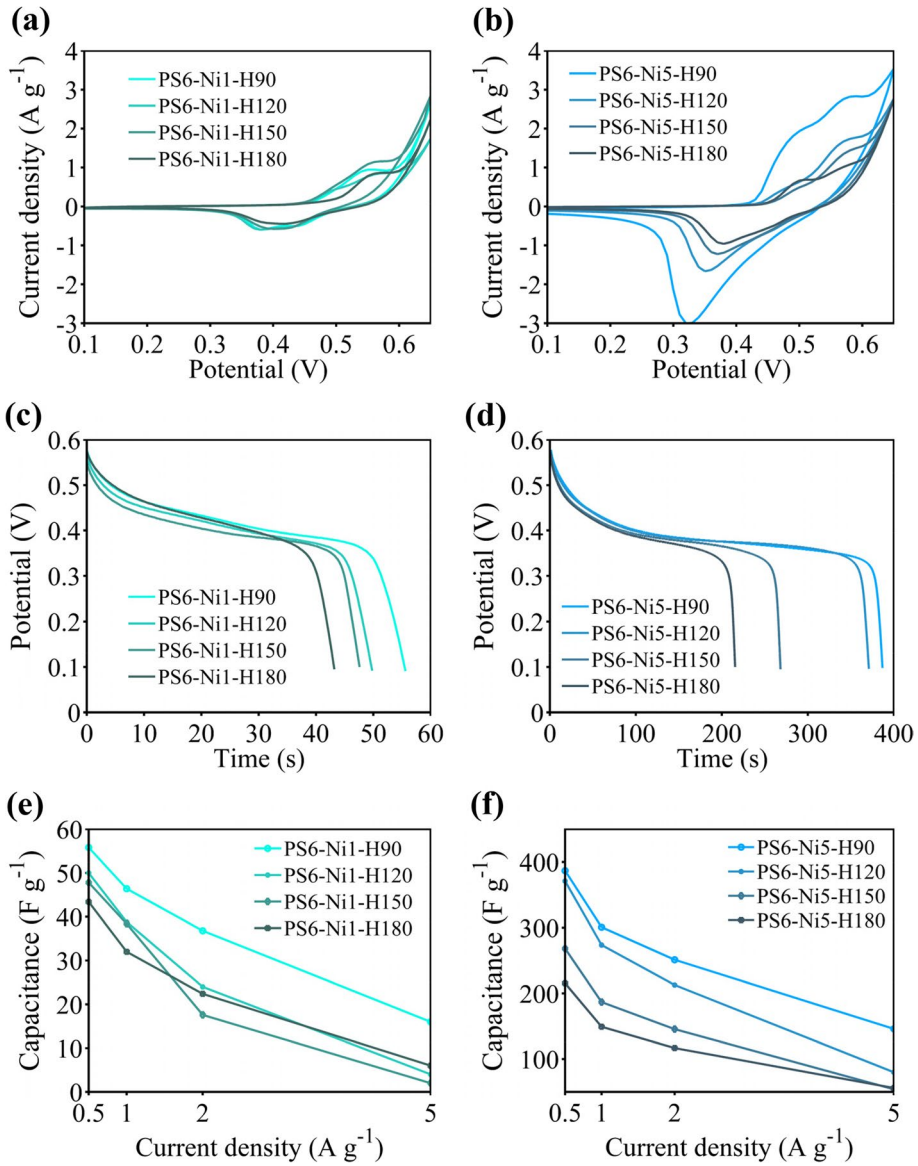

Fig. 2 The CV curves, electric discharge curves and the specific capacitance at different current density from 0.5 to 5 A g^{-1} for the pseudo-capacitive materials with different nickel content ((**a**, **c** and **e**): 100 mg g^{-1}, (**b**, **d** and **f**): 500 mg g^{-1}) and hydrothermal temperature. The CV curves were measured at 5 mV s^{-1} in a three-electrode system and the potential window from 0.1 V to 0.65 V (vs. Hg/HgO). The electric discharge curves were measured at 0.5 A g^{-1} from 0.1 V to 0.6 V

3 Results and discussion

3.1 Dominant role of biochar-adsorbed Ni in capacitive performance

By comparing the electrochemical characteristics of the capacitive materials with high and low Ni content and Ni-free biochar, we demonstrate that Ni adsorbed by biochar plays a key role in electrochemical performance. Figure 2 shows the electrochemical characteristics of the pseudo-capacitive material produced from Ni-laden biochar. As can be seen from the CV curves, two distinct oxidation peaks were observed around 0.5 V and 0.55 V during the positive scan, while a weak reduction peak (~ 0.45 V) and a powerful reduction peak (~ 0.35 V) could be observed during the reverse scan (Fig. 2a and b). The two oxidation peaks at 0.4–0.6 V and the reduction peak at 0.3–0.4 V could be attributed to the electrochemical reaction between $Ni(OH)_2$ and NiOOH (Tang et al. 2014; Jiang et al. 2015; Xu et al. 2019). Another possible contribution might come from the functional groups and the endogenous minerals of biochar, which are reported

to be involved in faradic reactions, like -NH-, −COOH, −C=O, etc. (Oh et al. 2014; Yan et al. 2014; Chen et al. 2017). However, our following experimental data did not support the direct participation of biochar components in capacitive reactions.

It can be seen from Fig. 2a and b that the area of CV curves for the samples with high nickel content (500 mg g^{-1}) was much larger than that for the samples with low nickel content (100 mg g^{-1}). The higher Ni content leads to a remarkable pseudo-capacitance performance, indicating that Ni compounds play a dominant role in the faradaic reaction. The electric discharge curves measured at 0.5 A g^{-1} directly reflect the capacitance of materials (Rong et al. 2015). As seen in Fig. 2c and d, the capacity of samples after hydrothermal treatments (90 °C, 120 °C, 150 °C, and 180 °C) showed a significant variation between high Ni content (approximate 210–390 F g^{-1}) and low Ni content (approximate 43–56 F g^{-1}). The discharge time of the high Ni samples was much longer (200–400 s) than those with low Ni content (40–60 s) (Fig. 2c and d). As the current density increased from 0.5 A g^{-1} to 5 A g^{-1}, the capacitance of the high Ni content biochar material decreased from around 200–400 F g^{-1} to 100–200 F g^{-1}, while the low Ni content biochar decreased from 40 to 60 F g^{-1} to 10–20 F g^{-1} (Fig. 2e and f). These results suggest that Ni adsorbed by biochar plays a crucial role in the electrochemical performance of the reclaimed biochar.

To clarify the effect of the hydrothermal process on the original biochar without adsorbed Ni, the control sample of original biochar was directly used for hydrothermal treatment for 4 h at 180 °C (PS6-H180). Compared the original biochar before hydrolysis (PS6) and after hydrolysis (PS6-H180), they had two reduction peaks with specific capacitances of 17.2 F g^{-1} and 7.4 F g^{-1}, respectively, according to the discharge curve with a current density of 0.5 A g^{-1} (Fig. S1). The low pseudo-capacitance indicated that the metal-free biochar could not be used for the production of faradic capacitor directly.

We also find that the area of CV curves and discharge time of PS6-H180 are much lower than those of the original biochar (PS6), suggesting that the hydrothermal treatment is unexpectedly detrimental to the production of the capacitive materials from the biochar alone without metals loading. Previous work also suggests that the hydrothermal process interferes with the faradic reactions of the biochar (Song et al. 2019). The most likely reason is that hydrothermal treatment leads to the hydrolysis of functional groups and the dissolution of metal oxides in biochar, which are involved in the faradaic reaction, although their contribution is not significant (Oh et al. 2014; Song et al. 2019). The results validate that the Ni in electroplating plant wastewater could be recycled by adsorption and subsequent hydrothermal treatment of biochar as a capacitive carrier, while the functional groups and minerals of biochar contributed little to the faradaic reaction.

3.2 Low hydrothermal temperature, high capacitive performance

The capacitance of the materials was found to decrease with the increase of the hydrothermal temperature for both high and low nickel concentrations, and the effect of temperature was more considerable for samples with high Ni content than for those with low Ni content (Fig. 2). As shown in Fig. 2b, the area of CV curves for PS6-Ni5-H90 was much larger than the other samples produced at 120–180 °C; Fig. 2c, d shows that the discharge time decreased to a large extent as the hydrothermal temperature increased; Fig. 2e, f shows that the capacitance of the samples with low Ni content (PS6-Ni1-H90, 120, 150, 180) was 55.6, 49.8, 47.6 and 43.2 F g^{-1}, at 0.5 A g^{-1} respectively. Those data with high Ni content (PS6-Ni5-H90, 120, 150, 180) was 386.7, 371.0, 268.2, and 215.4 F g^{-1}, respectively. Therefore, the highest capacitance of 386.7 F g^{-1} was achieved with the material of 500 mg g^{-1} nickel content and 90 °C hydrothermal temperature (PS6-Ni5-H90).

Further characterization for the materials with nickel concentration of 500 mg g^{-1} was carried out to explore its more electrochemical properties as energy storage materials. The cycling stability of pseudo-capacitive material was evaluated by the capacitance retention after 1000 charge-discharge cycles at 2 A g^{-1}. Results showed that the hydrothermal temperature had a slight influence on the cycling stability of the samples, and higher treating temperature led to higher cycling stability. For instance, for the materials produced at 90 °C, 120 °C, 150 °C and 180 °C, the cycling rates corresponded to 79.2%, 83.5%, 86.4% and 87.2%, respectively (Fig. 3a). The specific capacity loss of sample prepared at 90 °C had already reached more than the acceptable 20% (Chaari et al. 2011; Liu and Li 2020), thus this study only explored the temperatures above 90 °C.

The electron transfer impedance of four samples was measured from the impedance spectrum (Fig. 3b) (Wang et al. 2013). The equivalent series resistance (ESR) was calculated from the X-intercept of the impedance spectrum in the high-frequency region, which takes the resistance of current collector, the interconnection between current collector and capacitive material, the pseudo-capacitive materials, and electrolyte into consideration (Wei and Yushin 2011). The ESR of the electrode was stabilized in 2.2–2.3 Ω

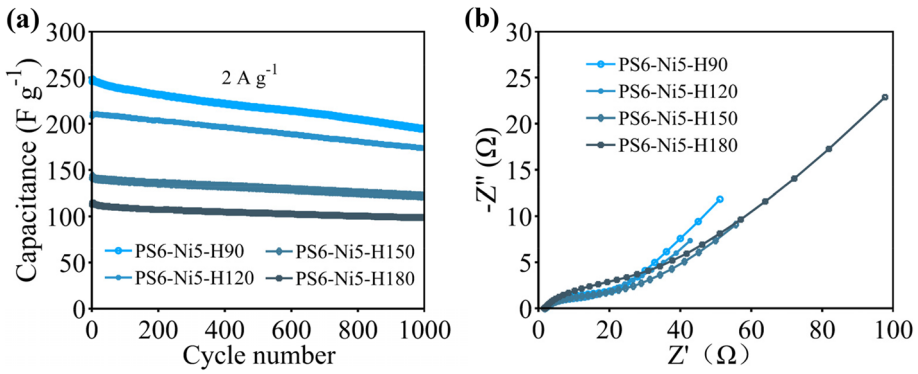

Fig. 3 The cycling stability (**a**) atthe current density of 2 A g^{-1} and Nyquist plot (**b**) were measured from 0.01 Hz to 10 kHz at 5 mV with the nickel content of 500 mg g^{-1}

Table 1 The cycling stability and electrochemical properties measured by EIS

Sample	ESR (Ω)	Rct(Ω)	Retention after 1000 cycle (%)
PS6-Ni5-H90	2.37	9.19	79.2
PS6-Ni5-H120	2.23	6.62	83.5
PS6-Ni5-H150	2.27	9.63	86.4
PS6-Ni5-H180	2.21	11.19	87.2

EIS Electrochemical impedance spectroscopy, *ESR* Equivalent series resistance, *Rct* Charge-transfer resistance

(Table 1). The charge-transfer resistance (Rct) was estimated with the circuit model of R(C(RW))(C) (Wang et al. 2015; Teng et al. 2017). Unlike the layer capacitive materials in our previous work (Li et al. 2021), the charge-transfer resistance (Rct) of pseudo-capacitive material was higher than that of the layer capacitor, indicating that the electron was difficult to transfer from the electrode surface to the connected ions in the electrolyte (Murali et al. 2019). With all aspects being taken into consideration, regarding capacitance performance, heating cost, cycling stability, and lower Rct, the 90 °C hydrothermal treatment was still the preferred condition.

Based on the electrochemical properties of these materials clarified above, the following issues should be further characterized: probing the crystal structure and morphology of $Ni(OH)_2$; determining the evolution of the carbon structure of the biochar; exploring the interactions between $Ni(OH)_2$ and carbon skeleton. All of these characterizations would allow us to gain insights into the role of Ni and carbon in the conversion of Ni-laden biochar into the pseudo-capacitive materials.

3.3 Homogeneously dispersed $Ni(OH)_2$ crystals on carbon surface

The XRD patterns of the pseudo-capacitive materials were presented in Fig. 4a and b. Accompanied with a small amount of graphite structure ($2\theta \approx 26.5°$), the nickel in the pseudo-capacitive materials mainly existed as the form of $Ni(OH)_2$ (PDF#03–0117). Moreover, the higher the hydrothermal temperature, the stronger the XRD peak of $Ni(OH)_2$ was observed, consistent with previous studies (Jiang et al. 2015). It is also evident from Fig. S2a, b, and Fig. 5 that the hydrothermal temperature has a direct effect on the grain size and shape of $Ni(OH)_2$. According to the simulation based on Scherer formula (Bharath et al. 2019), the grain sizes of PS6-Ni5-H90, PS6-Ni5-H120, PS6-Ni5-H150, and PS6-Ni5-H180 were 13.0 nm, 9.5 nm, 15.0 nm, and 16.1 nm, respectively. Among them, PS6-Ni5-H90 and PS6-Ni5-H120 showed a smaller size, while PS6-Ni5-H180 had the largest grain size. It is speculated that the high hydrothermal temperature leads to a relatively long cooling process, which induces the formation of a larger $Ni(OH)_2$ grain size. This phenomenon was consistent with the Rct calculated from EIS in Table 1, indicating that the smaller the grain size of $Ni(OH)_2$ leads to a lower Rct of the capacitor material, as in the previous research of RuO_2 (Li et al. 2018). In Fig. S2a and b, it can be found that the XRD peaks (102), (110), and (111) of $Ni(OH)_2$ showed the same trend in intensity with the increase of the temperature, while the main peaks (001), (100) and (101) have different trends at 120 °C. This indicates that lower temperatures of 90 °C and 120 °C are better than higher temperatures to produce the capacitive materials with smaller grain sizes and lower Rct.

The morphology of the capacitive materials was exhibited by SEM images shown in Fig. 5. As the samples

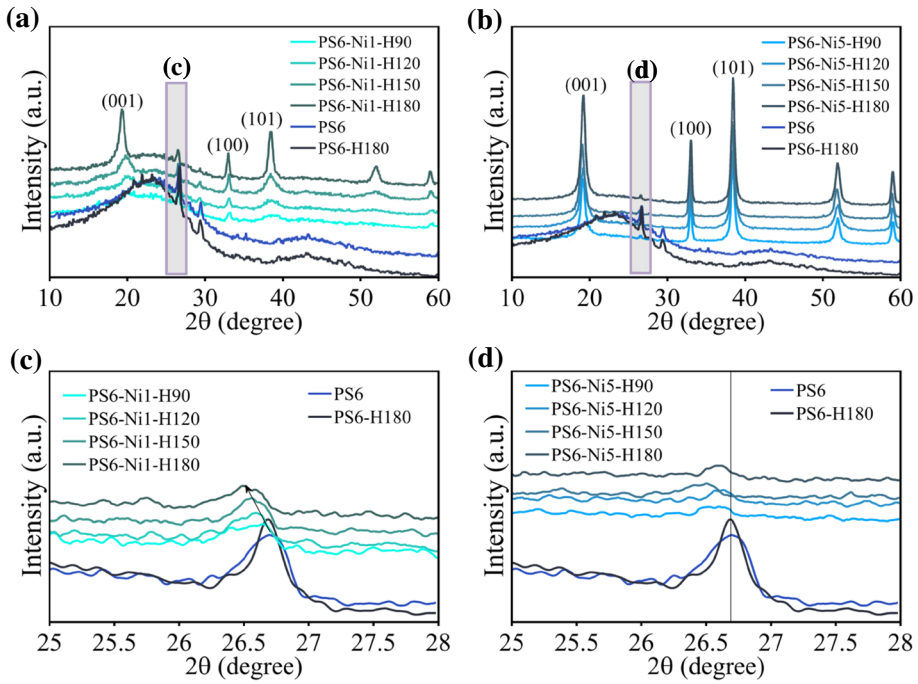

Fig. 4 XRD patterns for pseudo-capacitive materials with nickel content of 100 mg g^{-1} (**a**) and 500 mg g^{-1} (**b**); (**c** and **d**) The changes of graphite peaks in XRD pattern for PS6, PS6-H180 and pseudo-capacitive materials

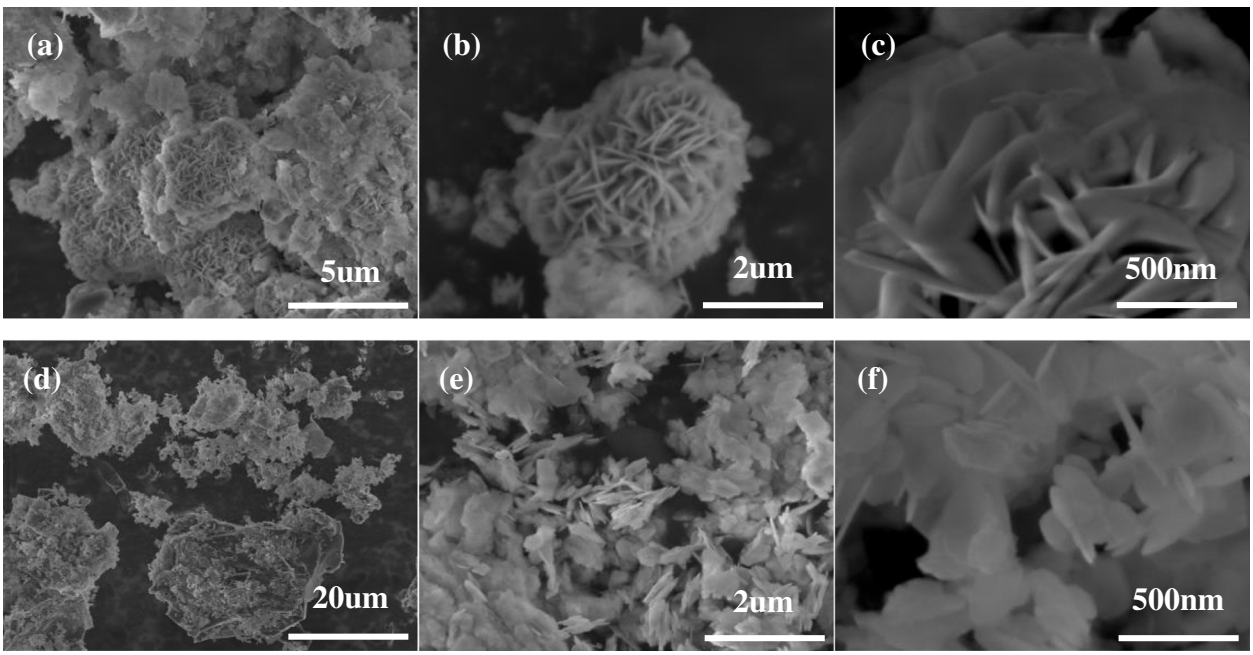

Fig. 5 SEM images of PS6-Ni5-H90 (**a**, **b**& **c**) and PS6-Ni5-H180 (**d**, **e** & **f**)

prepared at lower temperatures (90 °C, 120 °C) exhibited closer properties and so were those prepared at higher temperatures (150 °C, 180 °C), the SEM measurement was only carried out for PS6, PS6-H180, PS6-Ni5-H90 and PS6-Ni5-H180. The homogeneously dispersed flower-like $Ni(OH)_2$ was obtained in PS6-Ni5-H90 (Fig. 5a, b, and c),

and the nano lamellar structure of $Ni(OH)_2$ was observed in PS6-Ni5-H180 (Fig. 5d, e and f). With the increase of the hydrothermal temperature, the cyclic stability of the material increased slightly, which was related to the thicker crystal structure and the grain size of $Ni(OH)_2$ (Zhang et al. 2019b). Therefore, $Ni(OH)_2$ crystal at the carbon surface with uniform distribution could be prepared at a low temperature of 90 °C, which was better for ion transfer in electrolyte than those produced at 180 °C. The results mean that more $Ni(OH)_2$ could participated in the faradic reaction during the charging and discharging process, leading to a better capacitance performance and cyclic stability.

3.4 Nickel-carbon interaction enhanced the electrochemical stability of $Ni(OH)_2$

The interaction between nickel and carbon in the hydrothermal regime can be inferred from the various functional groups on the surface of the biochar, and the distance of the graphite layer in the biochar before and after the hydrothermal process (Oh et al. 2014; Chen et al. 2017). This can affect the electrochemical stability of $Ni(OH)_2$, which plays an important role in improving the potential applications of these capacitive materials. As can be seen from the FTIR spectra in Fig. S3, the peaks representing the -OH and Ni-O bonds of $Ni(OH)_2$ at 3640 cm^{-1} and 524 cm^{-1} (Lokhande et al. 2018) are detected more sharply for samples with 500 $mg\,g^{-1}$ nickel (Fig. S3b) than those with a Ni concentration of 100 $mg\,g^{-1}$ (Fig. S3a). It is clearly from Fig. S3b that the intensity of the peaks decreases as the hydrothermal temperature increases. This indicates that insoluble substances like $Ni(OH)_2$ dissolve first and disperse homogenously in the solution under the hydrothermal treatment.

Bending vibrations of small molecular functional groups such as N-H, C-N, etc. were detected at 1558 cm^{-1} (An et al. 2019; Silva et al. 2020) and 1385 cm^{-1} (Asyana et al. 2016), respectively. Distinct C-H bending vibration peaks at 875.5 cm^{-1} (Zhong et al. 2019) and C-H out-of-plane vibrations of 669 cm^{-1} (Trivedi et al. 2015; Iurchenkova et al. 2020) were also observed. All these peaks were in particular sharp for the samples of the original biochars (PS6 and PS6-H180) and the biochars with low Ni concentration (100 $mg\,g^{-1}$) (Fig. S3a), while the peaks seemed weak for the samples of 500 $mg\,g^{-1}$ nickel (Fig. S3b). Besides, all these peaks strength did not vary with the change of the hydrothermal temperature. Those peaks inferred that even in the hydrothermal system with relatively higher temperature and pressure, the functional groups on the biochar were stable and could resist the thermal decomposition. However, the peak (875.5 cm^{-1}) of PS6-Ni5-H180 is weaker than PS6 and PS6-H180, indicating that the catalytic effect of metal on the carbon structure.

As a result, under Ni catalysis, the functional groups on the surface of biochar were decomposed and converted into reactive carbon-containing small molecular fragments, such as hydroxyl radicals (Krysanova et al. 2019). So far, there is no definite evidence that Ni can form compounds with carbon in such relatively high-temperature and high-pressure solutions. However, their morphology and structures should have been reorganized and possibly fused, especially in the cooling phase with recrystallization of $Ni(OH)_2$. At different stages, including the warming, the holding, and the cooling, Ni and C may mutually wrap, as previously reported for Si and C in pyrolysis systems (Xiao et al. 2014).

In order to figure out the changes of carbon structure, the XPS was applied to prove the variation of functional groups and nickel-carbon interaction. A small amounts of metals like potassium and calcium were detected in the spectrum (Fig. S4). However, after the hydrothermal treatment, the peaks of metals in PS6-H180 were disappeared. Compared with PS6, the surface functional group of C-O and O-C=O decreased for PS6-H180, which led to a smaller capacitance (Fig. S1), from the high-resolution spectrum of C 1 s in Table S2, O 1 s in Table S3, Fig. 6 and Fig. S5. Furthermore, the lower nickel concentration (100 $mg\,g^{-1}$) could help the formation of C-O, while the higher concentration (500 $mg\,g^{-1}$) facilitated the decrease of C-O. Besides, the C=N increased after the hydrothermal treatment at 180 °C with 500 $mg\,g^{-1}$ nickel concentration, meaning that a part of the ammonium was added onto the surface of carbon skeleton. It was a coincidence that pyridinic and pyrrolic nitrogen increased for all the samples after hydrothermal treatment (Table S4). And the small amount of nickel (100 $mg\,g^{-1}$) could help the formation of pyridine-N-Oxide at 180 °C, while larger nickel particles from higher nickel concentration (500 $mg\,g^{-1}$) restrained it (Table S4). Those results suggested that large particles of nickel hydroxide could promote the erosion of carbon skeleton (C-O decreasing) and restrain the contact of ammonium and carbon, while small particles facilitate the formation of C-O and improve the interaction of ammonium and carbon skeleton.

3.5 Thermal stability of the materials characterized by combustion curves

To explore the binding mode of Ni and carbon skeletons, we have attempted to observe their microscopic morphology directly using combined energy dispersive spectroscopy and scanning/transmission electron microscopy (Li et al. 2021). However, since most of the carbon was amorphous carbon and the carbon skeleton was always

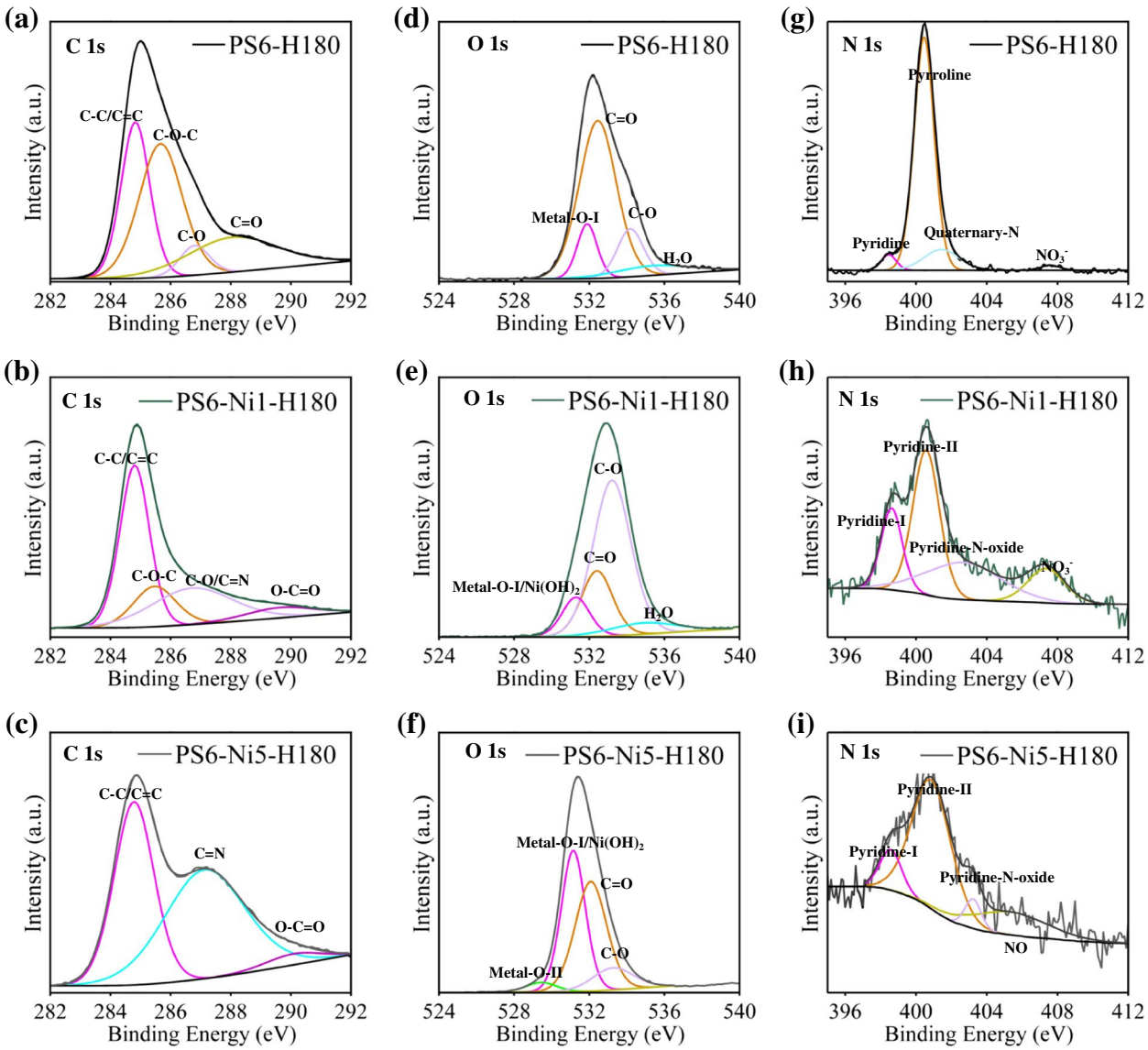

Fig. 6 High-resolution spectrum for C 1s, O 1s and N 1s of PS6-H180, PS6-Ni1-H180 and PS6-Ni5-H180 from XPS results and its relative components distribution

covered by $Ni(OH)_2$ crystal in Fig. 5 and Fig. S7, it was difficult to observe the nanoscale interaction. TGA was then employed to study the combustion process of the pseudocapacitive materials in air to analyze the nickel-carbon linkage. It is clear from the weight loss curves (Fig. 7a) and the derivative of thermogravimetric (DTG) curves (Fig. 7b) that all the Ni-laden biochar capacitive materials have a weight loss around 300 °C, while the nickel-free materials do not have this weight loss. For the dehydration stage of $Ni(OH)_2$, the weight loss of the samples prepared at 90 °C, 120 °C, 150 °C and 180 °C were 6.6%, 6.2%, 6.5% and 6.2% (245–320 °C), respectively.

The substantial weight loss of the material occurs at temperatures of 400–600 °C indicates the combustion of the carbon fraction. The bulk decomposition temperatures and combustion rates can reflect the thermal stability of the carbon skeleton in combination with Ni. Interestingly, there are significant deviations in combustion temperature and burning rate as well as heat flow between raw biochar (PS6) and hydrothermal treated biochar (PS6-H180). The former began to degrade from around 300 °C and ended at about 530 °C, while the latter initiated its degradation from 380 °C and finished at almost 600 °C (Fig. 7b and c). It

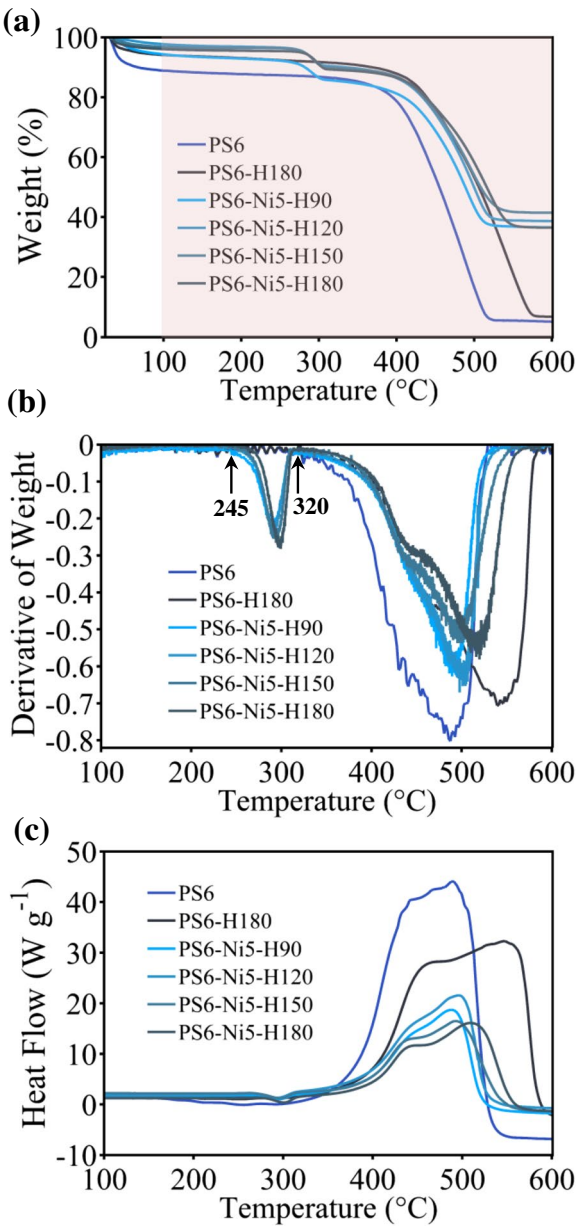

Fig. 7 (**a**) TGA curves for PS6, PS6-H180 and pseudo-capacitive materials with nickel content of 500 mg g^{-1}. (**b**) Derivative of TGA. (**c**) The heat flow in the TG measurement process

suggests that hydrothermal treatment can increase the combustion resistance of the carbon fraction to a large extent.

The capacitive materials obtained from Ni-laden biochars started the weight loss of carbon skeleton at higher temperatures and lower heat fluxes than those not loaded with nickel. Their combustion rates were significantly lower than those of PS6 and PS6-H180 (Fig. 7c). These curves can verify that the Ni-C cross-linked structure enhances the stability of the carbon skeleton. Moreover, the samples produced at higher hydrothermal temperatures (150 °C and 180 °C) showed a lagged combustion onset, longer combustion time, and lower heat flow than those produced at lower hydrothermal temperatures (90 °C and 120 °C). It can be concluded that increasing the temperature further enhanced the stability of the carbon skeleton.

It was noteworthy that the combustion process showed two exothermic peaks, one at around 450 °C, and the other at approximately 520 °C. They were especially obvious for the samples produced at higher temperatures (Fig. 7c). Moreover, the shape of the curves provided another information that the carbon skeleton burnt slowly at the first step near 450 °C, while it burnt quickly around 520 °C at the second step. It is speculated that the first combustion step was related to the dissociation of Ni and carbon facilitating the occurrence of the second combustion step (Fig. 7c). Therefore, the results of this section illustrated that hydrothermal treatment could significantly increase the thermal stability of the carbon skeleton (Kruse and Zevaco 2018), and the presence of Ni reinforced this thermal stability, which was especially obvious for the samples produced at a higher temperature.

3.6 Nickel inserted into biochar graphite layer improving its thermal stability

To figure out the subtle changes of carbon skeleton with Ni, we amplified the regions of XRD curves at 25–28 degrees (2θ) (Fig. 4a and b), as displayed in Fig. 4c and d. Comparing the peaks of PS6 and PS6-H180, we found that the peaks became sharper after the hydrothermal treatment at the same position, indicating that the hydrothermal treatment increased the graphite structure, while the distance of the graphite layer did not change. However, for the samples with Ni laden, the peaks of graphite kept shifting to the small angle with the rising of temperature, which meant that the presence of Ni promoted the expansion of graphite layer distance.

It is hypothesized that Ni could embed into the graphite layer of biochar, thus increasing its layer distance. It can be inferred from the contrary during analyzing the TGA results. As the graphitization degree of the samples was similar, if no substances were embedded in graphite layers, the combustion will be easier for the samples with a larger distance of graphite layer. However, the results in this study (Fig. 7) showed that the larger the distance of the

graphite layer was, the combustion process of the carbon skeleton would be more difficult, since the combustion need a higher temperature. Therefore, it can be inferred that the nickel was embedded into the graphite layer of biochar and protected the graphite structure, which led to the delay of combustion process and improved the overall stability of these pseudo-capacitive materials.

Previous studies have shown that metal particles can insert into graphite layers in extremely high-temperature environments (Huang et al. 2020). Presumably, this phenomenon is consistent with a previous study which showed that nickel hydroxide could insert into graphite layers during electrodeposition (Qu et al. 2017) and improve the stability of $Ni(OH)_2$. In this study, the firmly bonded nickel-carbon structure contributes to the overall electrochemical performance of the material. As a result of these discussions, exploring the combination mode and structure of nickel-carbon materials during hydrothermal processes is beneficial to achieve the synthesis of nickel-carbon structures with high electrochemical stability in the future.

4 Conclusions

In this study, the hydrothermal method was employed to recycle waste nickel-laden biochar for the production of the pseudo-capacitive materials. The highest capacitance of 386.7 $F\,g^{-1}$ with cyclic stability of 79.2% was obtained for the samples prepared at 90 °C, while samples prepared at 180 °C showed a capacitance of 215.4 $F\,g^{-1}$ with the stability of 87.2%. The results confirmed that Ni adsorbed on the biochar played a significant role in the electrochemical performance of the reclaimed biochar and that higher capacitance can be obtained at the hydrothermal temperature of 90 °C. Homogeneously dispersed flower-like $Ni(OH)_2$ crystals on the carbon surface could be observed in the sample at a low temperature of 90 °C, while higher temperature of 180 °C induced thicker flake structures of $Ni(OH)_2$. In this system, nickel-carbon interactions, such as nickel-catalyzed the hydrolysis of functional groups, as well as nickel inserting into biochar graphite layer, enhanced the electrochemical stability of $Ni(OH)_2$ and improved carbon thermal stability. This work provides a prospective strategy idea for recovering metals-laden biochar and using the interaction of metals and carbon to its maximum advantage. Further work can figure out the properties of real capacitor facilities from those materials. The cost and benefit for this strategy could also be considered.

Supplementary Information

The online version contains supplementary material available at https://doi.org/10.1007/s44246-022-00015-3.

Additional file 1: Table S1. Basic properties of the biochar. **Table S2.** XPS results for the C 1 s binding and its relative components distribution. **Table S3.** XPS results for the O 1 s binding and its relative components distribution. **Table S4.** XPS results for the N 1 s binding and its relative components distribution. **Fig. S1.** The CV curves (a) and electric discharge curves (b) of the control PS6 and PS6-H180 were measured with the scanning rate of 5 $mV\,s^{-1}$ and current density of 0.5 A g^{-1}. **Fig. S2.** The intensity for main peaks of $Ni(OH)_2$ from XRD spectrum at different hydrothermal temperature with two nickel contents (a: 100 $mg\,g^{-1}$, b: 500 $mg\,g^{-1}$). **Fig. S3.** FTIR spectra for PS6, PS6-H180 and the pseudo-capacitive materials with nickel content of 100 $mg\,g^{-1}$ (a) and 500 $mg\,g^{-1}$ (b). **Fig. S4.** XPS spectrums of PS6, PS6-H180 and the pseudo-capacitive materials with nickel loaded. **Fig. S5.** High-resolution spectrum for C 1 s, O 1 s and N 1 s of PS6, PS6-Ni1-H90 and PS6-Ni5-H90 from XPS results and its relative components distribution. **Fig. S6.** High-resolution spectrum for Ni 2p of the samples with nickel loaded from XPS results. **Fig. S7.** The detail SEM image of PS6-H180 (a, b, c), PS6-Ni5-H90 (d, e, f) and PS6-Ni5-H180 (g, h, i).

Authors' contributions

Deping Li: Methodology, Validation, Formal analysis, Investigation, Resources, Writing - Original Draft, Writing - Review & Editing. Jing Ma: Formal analysis, Writing - Review & Editing. Huacheng Xu: Resources, Writing - Review & Editing. Xiaoyun Xu: Resources, Supervision. Hao Qiu: Resources, Supervision. Xinde Cao: Conceptualization, Writing - Review & Editing, Supervision. Ling Zhao*: Conceptualization, Formal analysis, Writing - Review & Editing, Supervision, Project administration. The author(s) read and approved the final manuscript.

Funding

This work is supported by National Natural Science Foundation of China (No. 41877110).

Availability of data and materials

All data generated or analyzed during this study are included in this published article and its supplementary information files. The original datasets generated during the current study are available from the corresponding author on reasonable request.

Declarations

Competing interests

The authors declare that they have no known competing financial interests or personal relationships that could have appeared to influence the work reported in this paper.

Author details

[1]School of Environmental Science and Engineering, Shanghai Jiao Tong University, Shanghai 200240, China. [2]School of Environmental and Chemical Engineering, Shanghai University, Shanghai 200444, China. [3]State Key Laboratory of Lake Science and Environment, Nanjing Institute of Geography and Limnology, Chinese Academy of Sciences, Nanjing 210008, China. [4]China-UK Low Carbon College, Shanghai Jiao Tong University, Shanghai 201306, China.

Received: 15 April 2022 Accepted: 6 July 2022
Published online: 11 August 2022

References

An Q, Jiang YQ, Nan HY, Yu Y, Jiang JN (2019) Unraveling sorption of nickel from aqueous solution by $KMnO_4$ and KOH-modified peanut shell biochar: implicit mechanism. Chemosphere 214:846–854

Asyana V, Haryanto F, Fitri L, Ridwan T, Anwary F, Soekersi H (2016) Analysis of urinary stone based on a spectrum absorption FTIR-ATR. J Phys Conf Ser 694:012051

Bharath G, Rambabu K, Banat F, Hai A, Arangadi AF, Ponpandian N (2019) Enhanced electrochemical performances of peanut shell derived activated carbon and its Fe_3O_4 nanocomposites for capacitive deionization of Cr(VI) ions. Sci Total Environ 691:713–726

Cai W, Li Z, Wei J, Liu Y (2018) Synthesis of peanut shell based magnetic activated carbon with excellent adsorption performance towards electroplating wastewater. Chem Eng Res Des 140:23–32

Chaari R, Briat O, Deletage JY, Woirgard E, Vinassa JM (2011) How supercapacitors reach end of life criteria during calendar life and power cycling tests. Microelectron Reliab 51:1976–1979

Chen X, Paul R, Dai L (2017) Carbon-based supercapacitors for efficient energy storage. Natl Sci Rev 4:453–489

Cheng R, Xiang Y, Guo R, Li L, Zou G, Fu C, Hou H, Ji X (2021) Structure and Interface modification of carbon dots for electrochemical energy application. Small 17:2102091

Guo D, Zhang P, Zhang H, Yu X, Zhu J, Li Q, Wang T (2013) $NiMoO_4$ nanowires supported on Ni foam as novel advanced electrodes for supercapacitors. J Mater Chem A 1:9024–9027

Guo Z, Chen R, Yang R, Yang F, Chen J, Li Y, Zhou R, Xu J (2020) Synthesis of amino-functionalized biochar/spinel ferrite magnetic composites for low-cost and efficient elimination of Ni(II) from wastewater. Sc Total Environ 722:137822

Hao P, Ma X, Xie J, Lei F, Li L, Zhu W, Cheng X, Cui G, Tang B (2018) Removal of toxic metal ions using chitosan coated carbon nanotube composites for supercapacitors. Sci China Chem 61:797–805

Hu J, Tao P, Wang S, Liu Y, Tang Y, Zhong H, Lu Z (2013) Preparation of highly graphitized porous carbon from resins treated with Cr^{6+}-containing wastewater for supercapacitors. J Mater Chem A 1:6558–6562

Huang Q, Wang X, Li J, Dai C, Gamboa S, Sebastian PJ (2007) Nickel hydroxide/activated carbon composite electrodes for electrochemical capacitors. J Power Sources 164:425–429

Huang Z, Yao Y, Pang Z, Yuan Y, Li T, He K, Hu X, Cheng J, Yao W, Liu Y, Nie A, Sharifi-Asl S, Cheng M, Song B, Amine K, Lu J, Li T, Hu L, Shahbazian-Yassar R (2020) Direct observation of the formation and stabilization of metallic nanoparticles on carbon supports. Nat Commun 11:6373

Inyang M, Gao B, Yao Y, Xue Y, Zimmerman AR, Pullammanappallil P, Cao X (2012) Removal of heavy metals from aqueous solution by biochars derived from anaerobically digested biomass. Bioresour Technol 110:50–56

Iurchenkova AA, Fedorovskaya EO, Asanov IP, Arkhipov VE, Popov KM, Baskakova KI, Okotrub AV (2020) MWCNT buckypaper/polypyrrole nanocomposites for supercapasitor application. Electrochim Acta 335:135700

Jia H, Sun J, Xie X, Yin K, Sun L (2019) Cicada slough-derived heteroatom incorporated porous carbon for supercapacitor: ultra-high gravimetric capacitance. Carbon 143:309–317

Jiang C, Zhao B, Cheng J, Li J, Zhang H, Tang Z, Yang J (2015) Hydrothermal synthesis of $Ni(OH)_2$ nanoflakes on 3D graphene foam for high-performance supercapacitors. Electrochim Acta 173:399–407

Joseph L, Jun BM, Flora JRV, Park CM, Yoon Y (2019) Removal of heavy metals from water sources in the developing world using low-cost materials: a review. Chemosphere 229:142–159

Kılıç M, Kırbıyık Ç, Çepelioğullar Ö, Pütün AE (2013) Adsorption of heavy metal ions from aqueous solutions by bio-char, a by-product of pyrolysis. Appl Surf Sci 283:856–862

Kruse A, Zevaco T (2018) Properties of hydrochar as function of feedstock, reaction conditions and post-treatment. Energies 11:674

Krysanova K, Krylova A, Zaichenko V (2019) Properties of biochar obtained by hydrothermal carbonization and torrefaction of peat. Fuel 256:115929

Li D, Zhao L, Cao X, Xiao Z, Nan H, Qiu H (2021) Nickel-catalyzed formation of mesoporous carbon structure promoted capacitive performance of exhausted biochar. Chem Eng J 406:126856

Li X, Zheng F, Zhou DF, Luo YM, Li YF, Lu FH (2018) Stable RuO_2-based ternary composite electrode of sandwiched framework for electrochemical capacitors. Electrochim Acta 289:292–310

Lin L, Liu T, Liu J, Ji K, Sun R, Zeng W, Wang Z (2015) Synthesis of carbon fiber@nickel oxide nanosheet core–shells for high-performance supercapacitors. RSC Adv 5:84238–84244

Liu T, Li Y (2020) Addressing the Achilles' heel of pseudocapacitive materials: long-term stability. InfoMat 2:807–842

Lokhande PE, Pawar K, Chavan US (2018) Chemically deposited ultrathin α-Ni(OH)2 nanosheet using surfactant on Ni foam for high performance supercapacitor application. Mater Sci Energy Technol 1:166–170

Makgopa K, Bello A, Raju K, Modibane KD, Hato MJ (2019) Emerging nanostructured materials for energy and environmental science. Springer International Publishing, Switzerland, Cham, pp 247–303

Murali G, Harish S, Ponnusamy S, Ragupathi J, Therese HA, Navaneethan M, Muthamizhchelvan C (2019) Hierarchically porous structured carbon derived from peanut shell as an enhanced high rate anode for lithium ion batteries. Appl Surf Sci 492:464–472

Nwanya AC, Ndipingwi MM, Mayedwa N, Razanamahandry LC, Ikpo CO, Waryo T, Ntwampe SKO, Malenga E, Fosso-Kankeu E, Ezema FI, Iwuoha EI, Maaza M (2019) Maize (Zea mays L.) fresh husk mediated biosynthesis of copper oxides: potentials for pseudo capacitive energy storage. Electrochim Acta 301:436–448

Oh YJ, Yoo JJ, Kim YI, Yoon JK, Yoon HN, Kim J-H, Park SB (2014) Oxygen functional groups and electrochemical capacitive behavior of incompletely reduced graphene oxides as a thin-film electrode of supercapacitor. Electrochim Acta 116:118–128

Patil UM, Lee SC, Sohn JS, Kulkarni SB, Gurav KV, Kim JH, Kim JH, Lee S, Jun SC (2014) Enhanced symmetric supercapacitive performance of $Co(OH)_2$ nanorods decorated conducting porous graphene foam electrodes. Electrochim Acta 129:334–342

Qu R, Zhen D, Shuihua T, Zhentao Z, Geir Martin H (2017) Facile preparation of layered $Ni(OH)_2$/graphene composite from expanded graphite. Int J Electrochem Sci 12:8833–8846

Rong Q, Long L-L, Zhang X, Huang Y-X, Yu H-Q (2015) Layered cobalt nickel silicate hollow spheres as a highly-stable supercapacitor material. Appl Energ 153:63–69

Silva LG, Péres AFS, Freitas DLD, Morais CLM, Martin FL, Crispim JCO, Lima KMG (2020) ATR-FTIR spectroscopy in blood plasma combined with multivariate analysis to detect HIV infection in pregnant women. Sci Rep 10:20156

Song M, Zhou Y, Ren X, Wan J, Du Y, Wu G, Ma F (2019) Biowaste-based porous carbon for supercapacitor: the influence of preparation processes on structure and performance. J Colloid Interf Sci 535:276–286

Sun X, Jiang Z, Li C, Jiang Y, Sun X, Tian X, Luo L, Hao X, Jiang Z-J (2016) Facile synthesis of Co_3O_4 with different morphologies loaded on amine modified graphene and their application in supercapacitors. J Alloy Compd 685:507–517

Tang Y, Liu Y, Yu S, Zhao Y, Mu S, Gao F (2014) Hydrothermal synthesis of a flower-like nano-nickel hydroxide for high performance supercapacitors. Electrochim Acta 123:158–166

Tao P, Hu J, Wang W, Wang S, Li M, Zhong H, Tang Y, Lu Z (2014) Porous graphitic carbon prepared from the catalytic carbonization of Mo-containing resin for supercapacitors. RSC Adv 4:13518–13524

Teng Y, Liu K, Liu R, Yang Z, Wang L, Jiang H, Ding R, Liu E (2017) A novel copper nanoparticles/bean dregs-based activated carbon composite as pseudocapacitors. Mater Res Bull 89:33–41

Trivedi M, Branton A, Trivedi D, Shettigar H, Bairwa K, Jana S (2015) Fourier transform infrared and ultraviolet-visible spectroscopic characterization of biofield treated salicylic acid and sparfloxacin. Nat Prod Chem Res 3:1000186

Wang C, Xu J, Yuen M-F, Zhang J, Li Y, Chen X, Zhang W (2014) Hierarchical composite electrodes of nickel oxide nanoflake 3D graphene for high-performance pseudocapacitors. Adv Funct Mater 24:6372–6380

Wang J-W, Chen Y, Chen B-Z (2015) A synthesis method of MnO_2/activated carbon composite for electrochemical supercapacitors. J Electrochem Soc 162:A1654–A1661

Wang L, Wang Y, Ma F, Tankpa V, Bai S, Guo X, Wang X (2019) Mechanisms and reutilization of modified biochar used for removal of heavy metals from wastewater: a review. Sci Total Environ 668:1298–1309

Wang Q, Cao Q, Wang X, Jing B, Kuang H, Zhou L (2013) A high-capacity carbon prepared from renewable chicken feather biopolymer for supercapacitors. J Power Sources 225:101–107

Wang Y, Zhang Y, Pei L, Ying D, Xu X, Zhao L, Jia J, Cao X (2017) Converting Ni-loaded biochars into supercapacitors: implication on the reuse of exhausted carbonaceous sorbents. Sci Rep 7:41523

Wei L, Yushin G (2011) Electrical double layer capacitors with activated sucrose-derived carbon electrodes. Carbon 49:4830–4838

Xiao X, Chen B, Zhu L (2014) Transformation, morphology, and dissolution of silicon and carbon in rice straw-derived biochars under different pyrolytic temperatures. Environ Sci Technol 48:3411–3419

Xu L, Zhang L, Cheng B, Yu J (2019) Rationally designed hierarchical $NiCo_2O_4$-C@$Ni(OH)_2$ core-shell nanofibers for high performance supercapacitors. Carbon 152:652–660

Xue Y, Gao B, Yao Y, Inyang M, Zhang M, Zimmerman A, Ro K (2012) Hydrogen peroxide modification enhances the ability of biochar (hydrochar) produced from hydrothermal carbonization of peanut hull to remove aqueous heavy metals: batch and column tests. Chem Eng J 200-202:673–680

Yan J, Wang Q, Wei T, Fan Z (2014) Recent advances in design and fabrication of electrochemical supercapacitors with high energy densities. Adv Energy Mater 4:1300816

Yang Q, Lu Z, Liu J, Lei X, Chang Z, Luo L, Sun X (2013) Metal oxide and hydroxide nanoarrays: hydrothermal synthesis and applications as supercapacitors and nanocatalysts. Prog Nat Sci 23:351–366

Yang X, Jiang Z, Fei B, Ma J, Liu X (2018) Graphene functionalized bio-carbon xerogel for achieving high-rate and high-stability supercapacitors. Electrochim Acta 282:813–821

Yang Y, Li L, Ruan G, Fei H, Xiang C, Fan X, Tour JM (2014) Hydrothermally formed three-dimensional nanoporous $Ni(OH)_2$ thin-film Supercapacitors. ACS Nano 8:9622–9628

Zhang L, Shi D, Liu T, Jaroniec M, Yu J (2019a) Nickel-based materials for supercapacitors. Mater Today 25:35–65

Zhang S, Yang Z, Gong K, Xu B, Mei H, Zhang H, Zhang J, Kang Z, Yan Y, Sun D (2019b) Temperature controlled diffusion of hydroxide ions in 1D channels of Ni-MOF-74 for its complete conformal hydrolysis to hierarchical $Ni(OH)_2$ supercapacitor electrodes. Nanoscale 11:9598–9607

Zhi M, Xiang C, Li J, Li M, Wu N (2013) Nanostructured carbon–metal oxide composite electrodes for supercapacitors: a review. Nanoscale 5:72–88

Zhong M, Zhao Y, Zhai J-R, Jin L-J, Hu H-Q, Bai Z-Q, Li W (2019) Effects of nickel additives with different anions on the structure and pyrolysis behavior of Hefeng coal. Fuel Process Tech 193:273–281

Publisher's Note